IEEE Access
Multidisciplinary | Rapid Review | Open Access Journal

Received January 8, 2020, accepted January 18, 2020, date of publication January 23, 2020, date of current version February 11, 2020.

Digital Object Identifier 10.1109/ACCESS.2020.2968928

Soft Actuator Model for a Soft Robot With Variable Stiffness by Coupling Pneumatic Structure and Jamming Mechanism

FENG-YU XU[1,3], FENG-YOU JIANG[1,4], QUAN-SHENG JIANG[2], AND YU-XUAN LU[1]

[1]Jiangsu Engineering Lab for IOT Intelligent Robots (IOTRobot), College of Automation, Nanjing University of Posts and Telecommunications, Nanjing 210003, China
[2]School of Mechanical Engineering, Suzhou University of Science and Technology, Suzhou 215009, China
[3]Nanjing Nanyou Institute of Information Technovation Co., Ltd., Nanjing 210003, China
[4]Jiangsu Key Laboratory for Elevator Intelligent Safety, Changshu Institute of Technology, Changshu 215500, China

Corresponding author: Feng-Yu Xu (xufengyu598@163.com)

This work was supported in part by the Joint Research Fund for Overseas Chinese, Hong Kong and Macao Young Scholars under Grant 61728302, in part by the National Natural Science Foundation of China under Grant 51775284, in part by the Primary Research and Development Plan of Jiangsu Province under Grant BE2018734, in part by the Six Talent Peaks Project in Jiangsu Province under Grant JY-081, and in part by the Foundation of Jiangsu Key Laboratory for Elevator Intelligent Safety under Grant JSKLESS201709.

ABSTRACT Current research into soft robots not only needs to improve their compliance, but also requires consideration of the real-time controllability of rigidity and flexibility. By combining the advantages of Pneu-Net structure and the driven jamming mechanism, we developed a soft actuator model for a soft robot with real-time variable stiffness. Firstly, the model of the soft actuator coupled with pneumatic structure and jamming mechanism was built. Secondly, we analyzed the pneumatically-driven structure by using the finite element method and researched the influences of pressure in cavities as well as shape and size of cavities on the performance of bending motion. On this basis, the pneumatically-driven structure was optimized. Finally, a prototype of the soft robot arm with variable stiffness was designed to carry out the experiment for verifying the variable stiffness of the soft actuator. Theoretical analysis and experimental results demonstrate that the soft robot can withstand a variable stiffness of between 0.025-0.138N/mm. In addition, the maximum elongation of the designed coupling mechanism can reach 25mm.

INDEX TERMS Soft actuator, robot with variable stiffness, particle jamming, three-dimensional printing.

I. INTRODUCTION

When interacting with the natural environment, traditional rigid robots are not compliant enough and have limited adaptability to the environment, which greatly limits their range of application. In recent years, robots made of soft materials have become a research hotspot [1]. Compared with rigid robots, soft robots have higher environmental adaptability, sensitivity, and flexibility and can absorb the energy produced by contact. Moreover, they interact with humans and can simulate continuous movement of biological systems.

Building an accurate model of motion for soft robots is extremely challenging. The difficulties are that actuator structures and materials are often non-linear and a soft actuator with a complex structure shows infinite degrees of freedom in theory [2]. Furthermore, theoretical analysis, numerical simulation and experimental methods are usually used for modelling [3].

(1) In terms of theoretical modelling, many scholars have established simplified models by utilising theoretical analysis to study deformation and stiffness characteristics of soft actuators [4]. For example, based on the piecewise constant curvature model, Saunder et al. studied the motion characteristics of an actuator [5]. Through use of Euler-bernoull beam theory, Shapiro *et al.* built the quasi-static model of a soft actuator [6]. By utilising the minimal potential energy method, Carmel et al. obtained the relationship between cavity pressure and deformation of a soft actuator [7]. Based on modelling using the piecewise constant curvature method, Jones established the forward and inverse kinematic models of a soft robot by directly correlating the classical Denavit-Hartenberg (D-H) form with a piece-wise constant (PCC)

The associate editor coordinating the review of this manuscript and approving it for publication was Ludovico Minati.

method [8]. In view of the shortcomings of design and modeling methods for soft robots in modularisation, researchers have effectively combined the finite element analysis with the kinematics modeling of soft robots, which can capture inherent high non-linear deformation of soft robots under the assumption of PCC model [9]–[11]. Wang et al. put forward a new triangular closed-chain soft rolling robot and established a state space model to simulate rolling state and continuous deformation of the robot [12]. Based on previous kinematic modelling, Tan *et al.* evaluated the uncertain poses of a soft robot driven by a flexible shaft by using an interval analysis method [13].

(2) Mathematical models built through theoretical analysis are complex, so some scholars analysed the deformation and stress of soft actuators by using finite element method. For instance, ShuiChi *et al.* simulated bi-directional motion of a soft actuator by employing finite element software [14]. Panagiotis *et al.* performed stress analysis on deformation process of an actuator by utilising finite element analysis software and deduced the contact force at the end through reaction force at a node on the edge of the end. In addition, according to finite element simulation results and experimental data [15], Gunjan *et al.* studied the effects of cavity shape and material characteristics on the bending performance of an actuator. By using the finite element method [16], Ganesha *et al.* investigated the influences of thickness of the side wall of a corrugated pipe on deflection performance of mechanism [17]. Meng *et al.* designed a pneumatic soft robot arm with three cavities and analysed the deformation thereof by applying the finite element method, which provides a reference for optimization of the design of the mechanism [18], [19].

(3) Researchers have conducted many tests on mechanisms with variable stiffness wherein, changes of stiffness were simulated by measuring resistance by changing displacement at the end of the mechanism which is then compared with a measured offset. Wei built a special experimental platform and fixed an actuator on the bracket to form a cantilever beam, while loads were hung on the other end to simulate the changes in stiffness of the mechanism through the ratio of offset at the end to load weight [20]. Allen proposed a bending test platform, with one end of an actuator fixed horizontally and the other in contact with a sensor mounted on a linear slide track and deduced variable stiffness value by comparing sensor reading with displacement of the sliding block, however, the above two platforms neglect the influences of gravity on such robots, so they are only suitable for the mechanisms with small self-weight [21]. Furthermore, Arjo fixed the soft actuator on the lift platform and hung the end of the actuator on a balancer through a haul rope, thus eliminating effects of gravity [22]. When the lifting platform slides downwards, the balancer also moves downwards to keep the mechanism in a horizontal state, so stiffness was simulated through the recorded drawing force of the haul rope and sliding distance, by utilising a stepper motor and a guide rail, Yang further improved the experimental platform for testing of such soft robots [23]. The two platforms have considered the influence of gravity on the experiment, and are suitable for experiments on the mechanisms with large self-weight. Brown proposed a positive pressure universal gripper based on the jamming of granular material. By using both positive and negative pressure. Brown demonstrate performance increases of up to 85% in reliability, 25% in error tolerance [24]. Mariangela summed up the semi-active approach which Inspired us much. In addtion, they experimentally characterized the stiffness trends through axial and lateral force-displacement measurements. The overall stiffness range was found to lie between 0.03 N/mm -0.072 N/mm [25]. Wei built a special experimental platform and fixed an actuator on the bracket to form a cantilever beam [20], while loads were hung on the other end to simulate the changes in stiffness of the mechanism through the ratio of offset at the end to load weight. The variable stiffness rang of the mechanism between 0.021 - 0.088 N/mm. Compared with the above variable stiffness jamming mechanism, our jamming mechanism has the characteristics of high precision of repeated positioning and the soft robot can withstand a variable stiffness of between 0.025 - 0.138 N/mm.

In addition, there are also many research on soft robot. Wang presents the design, modeling, and testing of a soft pneumatic glove with five segmented PneuNets bending actuators (SPBAs) made of elastomer [26]. Cianchetti combine flexible fluidic actuators to obtain multidirectional bending and elongation with a variable stiffness mechanism based on granular jamming which can bending 64°, but it can not elongate [27]. Compared with the above pneumatic mechanism, the max bending angle of our mechanism is 68.2°. In addition, the maximum elongation of our coupling mechanism can reach 25mm.

There are also many ways to model for soft robots. Bao proposed a kinematic model for TCP-based elastomer soft robots [28]. It has two main contributions. First, constant curvature assumption (CCA), the foundation in soft robots is conceptualized and the pioneering proof is constituted. Second, an innovative but foundational soft robot kinematic model is established based on CCA called constant curvature elastomer model (CCE). Zhang proposed a phenomenological modeling method to realize a mathematical model with high precision, limited calculation, and easy engineering applicability of the pipe-crawling soft robot [29]. Then, the prototype of the robot is fabricated with the optimal structural parameters selected by finite element simulations. The static identification experiment shows that the average errors of the extended length and output force are 0.51 mm and 0.28 N, respectively.

By combining the advantages of the Pneu-Net structure and driven jamming mechanism, we designed a soft actuator with real-time variable stiffness. The paper is structured as follows: Section 2 covers the structural model of the soft robot with variable stiffness; the pneumatically-driven structure is analysed by using the finite element method in Section 3; the prototype of the robot is described in Section 4; in Section 5 we describe the design of the test platform for

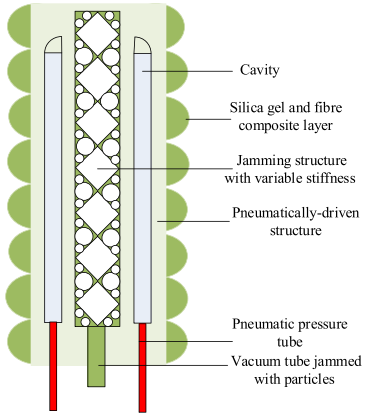

(a) Section view

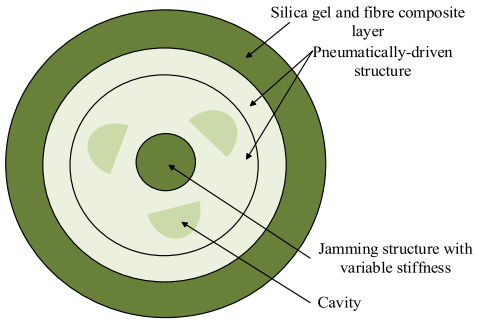

(b) Top view

FIGURE 1. Mechanism of unit actuator.

stiffness and completed the experiment for verifying stiffness under pneumatic drive conditions.

II. MODEL OF THE SOFT ACTUATOR WITH VARIABLE STIFFNESS

In the field of soft robots, previous studies have focused on improving compliance. Here, we designed a soft robot with variable stiffness with controllable stiffness and flexibility, that is, the robot is required to have high flexibility when moving and high stiffness when performing tasks. Based on the idea of modular design, the robot was built by disassembling the complex soft robot into soft actuators with a single module and then connecting them. The structure of unit module, as shown in Figure 1a consisted of a jamming mechanism with variable stiffness, cavities, a pneumatically-driven structure, a fibre composite layer, a pneumatic pressure tube and a vacuum tube jammed with particles.

The soft actuator comprised three layers: the jamming mechanism with variable stiffness was found in the innermost layer and its bottom was connected with the vacuum tube jammed with particles. The middle layer showed the pneumatically-driven structure (Figure 1b). Moreover, the silica gel-fibre composite structure in the outermost layer could limit excessive expansion of the pneumatic structure.

A. THE JAMMING MECHANISM WITH VARIABLE STIFFNESS

The jamming mechanism with variable stiffness is improved based on the existing jamming mechanism containing small particles and is cylindrical. The specific structure is shown in Figure 2. The bottom of the structure was connected with the external vacuum pump through the vacuum tube jammed with particles, and the outside was wrapped in a thin film. The space formed by the thin film was filled with a number of diamond-shaped skeletons, which were connected by flexible rope. Large spherical particles connected by strings were embedded between two adjacent diamond-shaped skeletons after the springs were tightened and the gap was filled with fine particles.

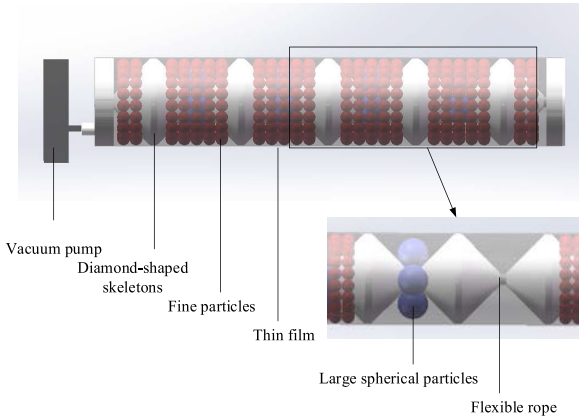

FIGURE 2. Jamming mechanism combining large and small particles.

The working principle is as follows: after applying vacuum pressures, fine granules in the space formed by the film change from fluid state to solid state. In the solid state, the large spherical particles and diamond-shaped skeletons were integrated into one after sealing the film, while gaps between large spherical particles and joint skeletons were filled with fine particles. When the mechanism moved, the large spherical particles were always embedded between the joint skeletons and were not randomly scattered. The stiffness of the robot was adjusted by controlling the hardness of the vacuum in the film. The jamming mechanism overcomes the shortcoming of jamming mechanism with small particles which causes uncertain position and even positioning error due to particle recombination during motion.

B. PNEUMATICALLY-DRIVEN STRUCTURE

The pneumatically-driven structure was made of elastic materials. Three cavities, at angles of 120° (allowing bending in any direction) were set around its circumference and the bottoms of the cavities were connected to the pneumatic pressure tube (Figure 3a). When loading with a single cavity, the mechanism bent in a single direction and bending deformation are related to the gas volume loaded in the cavity.

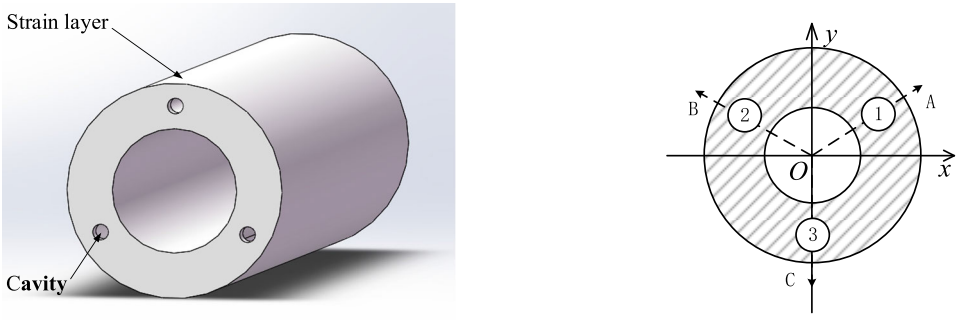

(a) Structural model (b) Motion model

FIGURE 3. Pneumatically-driven structure of the soft actuator.

When two or above cavities were inflated at the same time, this model could be simplified into three vectors at 120° to each other and each vector is correlated with gas volume in the corresponding cavity. The coordinate system shown in Figure 3b was built in the fixed end of the mechanism and bending effects of each cavity after loading are equivalent to three vectors, *i.e.* $\vec{OA}$, $\vec{OB}$ and $\vec{OC}$, and the bending effect is equivalent to the sum of the three vectors when loaded with multiple cavities.

$$\vec{OP} = \mathrm{a}\,\vec{OA} + \mathrm{b}\,\vec{OB} + \mathrm{c}\,\vec{OC} \tag{1}$$

If it is intended to bend the mechanism in the direction of point P, specific deformation of each cavity can be obtained by using Formula (1) for decomposition and then the mechanism is driven in any direction by controlling the inflated volume in each cavity.

C. SILICA GEL AND FIBRE COMPOSITE LAYER

When a large amount of air was injected in the cavities, the outer walls might over-expand, generating balloon effects. The silica gel and fibre composite layer, appearing as rings in the external structure, was made of materials with a large elastic modulus. Multiple single-ring fibres were inserted onto the surface of the actuator. Such a limited fibre structure only limits the excessive expansion of the actuator in the radial direction, while only slightly affecting stretch, compression, and bending in the axial direction. Meanwhile, such a fibre composite structure can increase the viscous force when grasping objects, provide greater endpoint force, and show high bending efficiency.

III. FINITE ELEMENT ANALYSIS OF THE SOFT ACTUATOR WITH VARIABLE STIFFNESS

The finite element analysis can approximately describe motion and shape of the pneumatic soft structure under different conditions, which provides guidance for parameter optimisation and structure design. We built the model by using the finite element method to simulate and analyse the pneumatic loading process of the pneumatic soft robot.

A. PARAMETER SETTING

Without affecting the accuracy of the analysis of the mechanism, the air inlet of the pneumatic soft actuator can be simplified and some parts exerting little influence on the mechanism can be omitted.

The soft actuator made of silica gel, a super-elastic material, is generally described by the constitutive model. Based on observations by Ogden of the elastic characteristics of rubber, the model can accurately describe large deformation of non-linear materials by predicting mechanical behaviours, such as stretch and shear of flexible materials through unidirectional tension and compression tests [30]. This strain-energy function is shown as follows:

$$\mathrm{W}_{Ogden} = \sum_{i=1}^{N} 2\mu_{\mathrm{i}}/\alpha_i^2 \left(\lambda_1^{\alpha_n} + \lambda_2^{\alpha_n} + \lambda_3^{\alpha_n} - 3\right) + \sum_{i=1}^{N} \frac{1}{D_i} (J-1)^{2i} \tag{2}$$

where, $\mathrm{W}_{\mathrm{Ogden}}$ represents the strain-energy density; μ_{i} and α_{i} are material parameters; J, λ_{i} and N indicate the ratio of deformed volume to the undeformed volume, the elongation when the mechanism is mainly tensile, and the number of terms in the strain-energy function. Moreover, $\mathrm{D_i}$ denotes the coefficient of volume deformation of the material and D = 0 if the material is incompressible.

By utilising the strain energy density function of the Ogden model, the silica gel materials were set as hyper-elastic bodies and the third-order Ogden model was used to describe the hyper-elastic mechanical behaviour of the material (Table 1) [31].

B. SIMULATION ANALYSIS AND PARAMETER OPTIMIZATION WHEN LOADING WITH A SINGLE CAVITY

The soft actuator was mainly subjected to external force of fixture at the end and its self-weight. Firstly, the three-dimensional parts of the soft actuator were introduced into ABAQUS (Figure 4a), and then the material properties were defined as elastomers. The potential energy of strain followed a third-order Ogden model. Any one cavity of the pneumatically-driven structure was loaded to 20kPa to simulate external pressure. The model constraints are as follows:

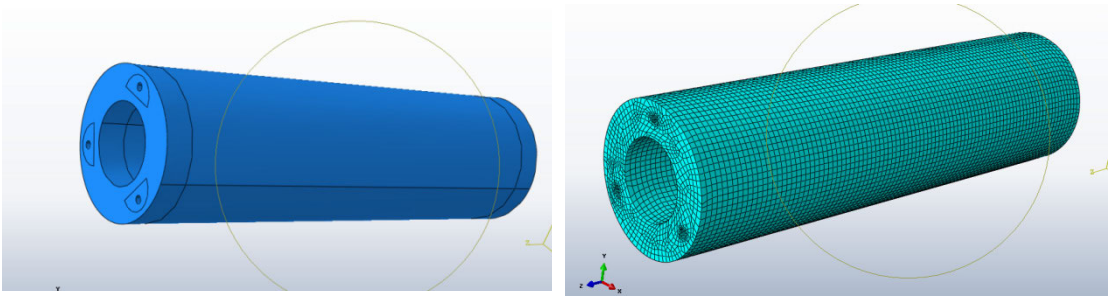

(a) Simplified model (b) Mesh generation

FIGURE 4. Finite element model of the soft actuator.

TABLE 1. Parameters used in the Ogden model.

Coefficient μ_i	Coefficient α_i	Coefficient Di
μ_1=0.024361	α_1=1.7138	D_1=3.2587
μ_2=6.6703×10^{-5}	α_2=7.0679	D_2=0
μ_3=4.5381×10^{-4}	α_3=-3.3659	D_3=0

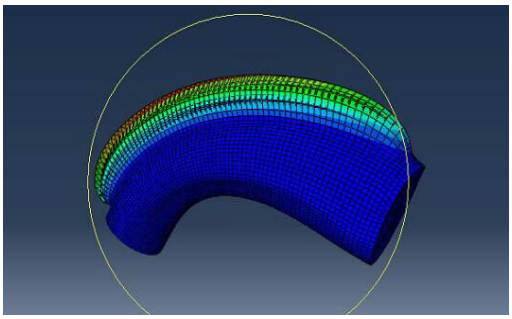

FIGURE 5. Cloud picture of total deformation when loading with a single cavity in the soft actuator.

the round surface of the air inlet end was completely fixed. The mesh is shown in Figure 4b.

The structure of the soft actuator was then defined with fixed constraints and load and the stress and strain were finally obtained and analysed. By applying different pressures on the pneumatic structure, the deformation patterns are displayed in Figure 5.

The bending angle is a key index of the soft actuator; by using the finite element method, an air pressure of 0-20kPa was applied to a single cavity in the soft actuator to induce bending deformation at the end. The bending angle of the mechanism is shown in Figure 6. It can be seen that the larger the gas pressure, the larger the bending angle of the soft actuator. When the change in gas pressure is the same, the bending angle increases.

By using the finite element method, semi-circular cavities with different wall thicknesses were analysed. By applying a pressure of 4-20kPa in intervals of 2kPa, the relationship

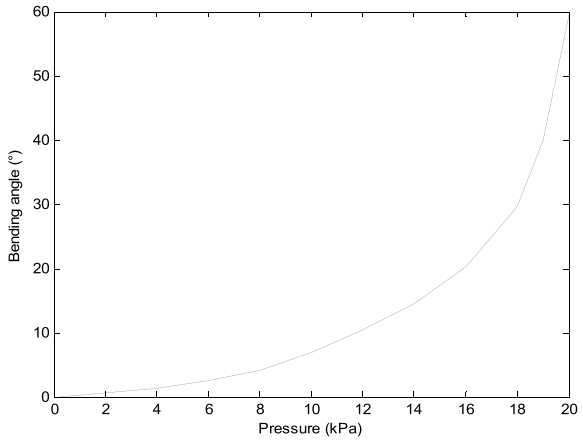

FIGURE 6. The relationship between bending angle and pressure.

between bending angle and pressure under different wall thicknesses was obtained (Figure 7). The figure demonstrates that the smaller the wall thickness of the cavities, the better the bending deformation performance obtained under the same pressure. Furthermore, as the pressure is increased, the smaller the wall thickness of the cavities, the larger the difference in bending angles under the same pressure.

C. SIMULATION ANALYSIS WHEN LOADING WITH TWO CAVITIES

Any two cavities in the soft actuator were set to the same pressure and the end face for inflation was fixed. The simulation is presented in Figure 8a and the maximum von Mises stress on the soft actuator is 0.3018MPa.

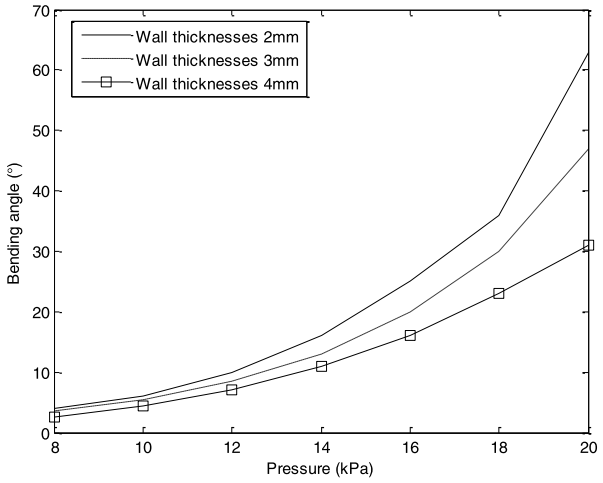

FIGURE 7. The relationship between bending angle and pressure under different wall thicknesses.

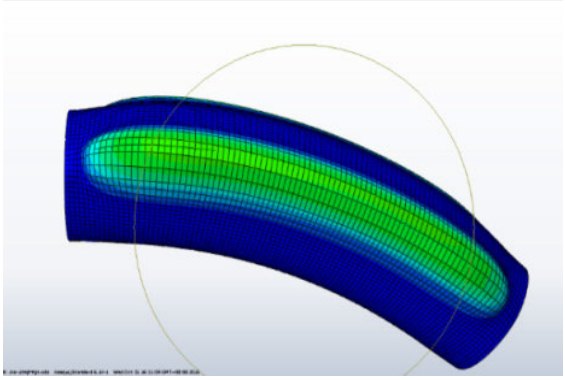

(a) Cloud picture of total deformation

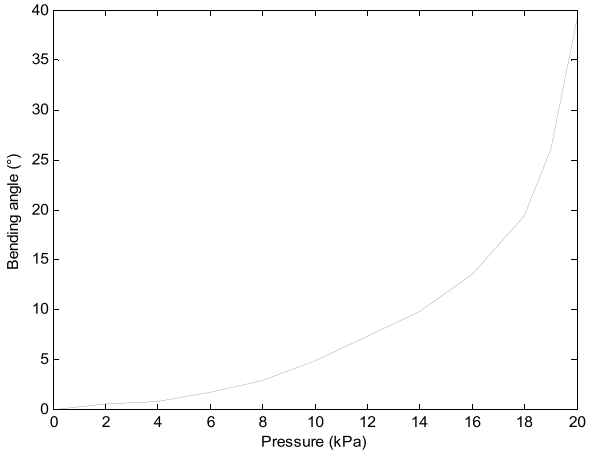

(b) The relationship between bending angle and pressure

FIGURE 8. Simulation results when loading with double cavities.

By setting the cavity pressures to 0-20kPa, simulation analysis was performed. By establishing the reference points at the end of the mechanism and setting the field output, the offset at the end of the mechanism was obtained, thus acquiring the relationship between bending angle and pressure (Figure 8b). After inflating the double cavities in the pneumatically-driven structure, deformation at the end increases with the rise of inflation time and the maximum bending angle is 39.234°. Meanwhile, in the same time interval, the increment of tensile deformation at the end increases continuously.

D. SIMULATION ANALYSIS WHEN LOADING WITH THREE CAVITIES

The three cavities of the soft actuator were set to deliver an air pressure of 20kPa and the end-face for inflation was fixed. The total deformation is demonstrated in Figure 9a. The reference points were set at the end of the mechanism and field output was set to obtain the relationship between the elongation at the end and pressure (Figure 9b): the tensile deformation at the end increases with increasing inflation and the maximum tensile deformation reached 28.234mm. At the same time, the change of tensile deformation at the end constantly increases within the same time interval.

IV. MANUFACTURING PROCESS OF SOFT ROBOT

To verify variable stiffness of the soft actuator, a soft robot prototype was made; meanwhile a test platform was built. The SI unit for magnetic field strength H is A/m. However, if you wish to use units of T, either refer to magnetic flux density B or magnetic field strength symbolized as $\mu_0 H$. Use the center dot to separate compound units, e.g., "A·m^2."

A. MANUFACTURE OF THE ROBOT MACHINE

1) MANUFACTURE OF SOFT ROBOT WITH VARIABLE STIFFNESS

In accordance with the structural model proposed in Section 2, the main components of the soft robot, such as plugs and diamond-shaped skeletons were designed and manufactured through 3D printing. Parts, such as a ventilation pipe, a flexible rope, a thin film, and particles for filling were prepared. An elastic rubber band with width of 2.8mm was used as the flexible rope and thin film was made of PE with a thickness of 0.24mm. Moreover, corundum particles with a radius of 3mm were used for filling the model.

The specific assembly process is as follows: the flexible rope was passed through the centre holes of the plug and the diamond-shaped skeletons and was then glued and fixed at equal intervals. Furthermore, the ventilation pipe was connected to convex slot cut in the plugs for ventilation purposes. After that, the diamond-shaped skeletons of the component were successively packed with the thin film and particles were packed therein. Finally, two ends were sealed with silicone glass sealants to make the prototype.

2) PREPARATION OF THE PNEUMATICALLY-DRIVEN STRUCTURE

The silicone materials are mainly Ecoflex 0030 silicone and Dragon skin 10 silicone produced by smoot-on company. Ecoflex 0030 silica gel has A shao's hardness of 30A and A mixture viscosity of 3000cps. It is divided into two groups

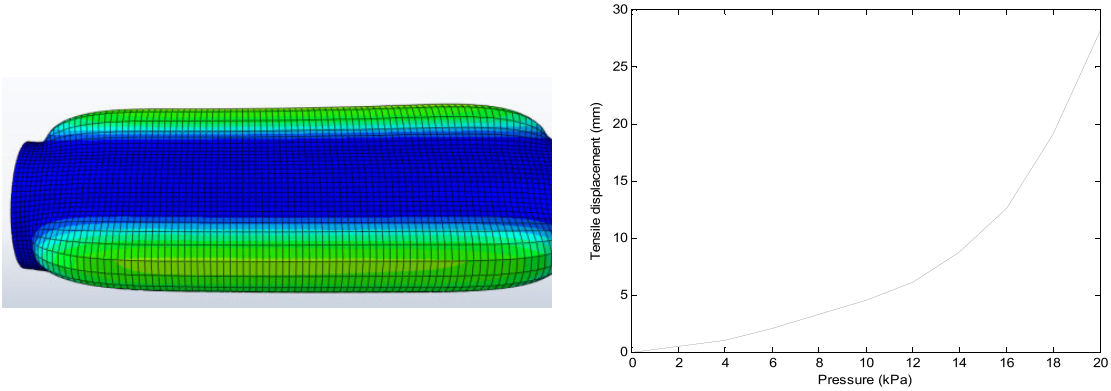

(a) Cloud picture of total deformation

(b) Tensile displacement with three cavities

FIGURE 9. Simulation results when loading with three cavities.

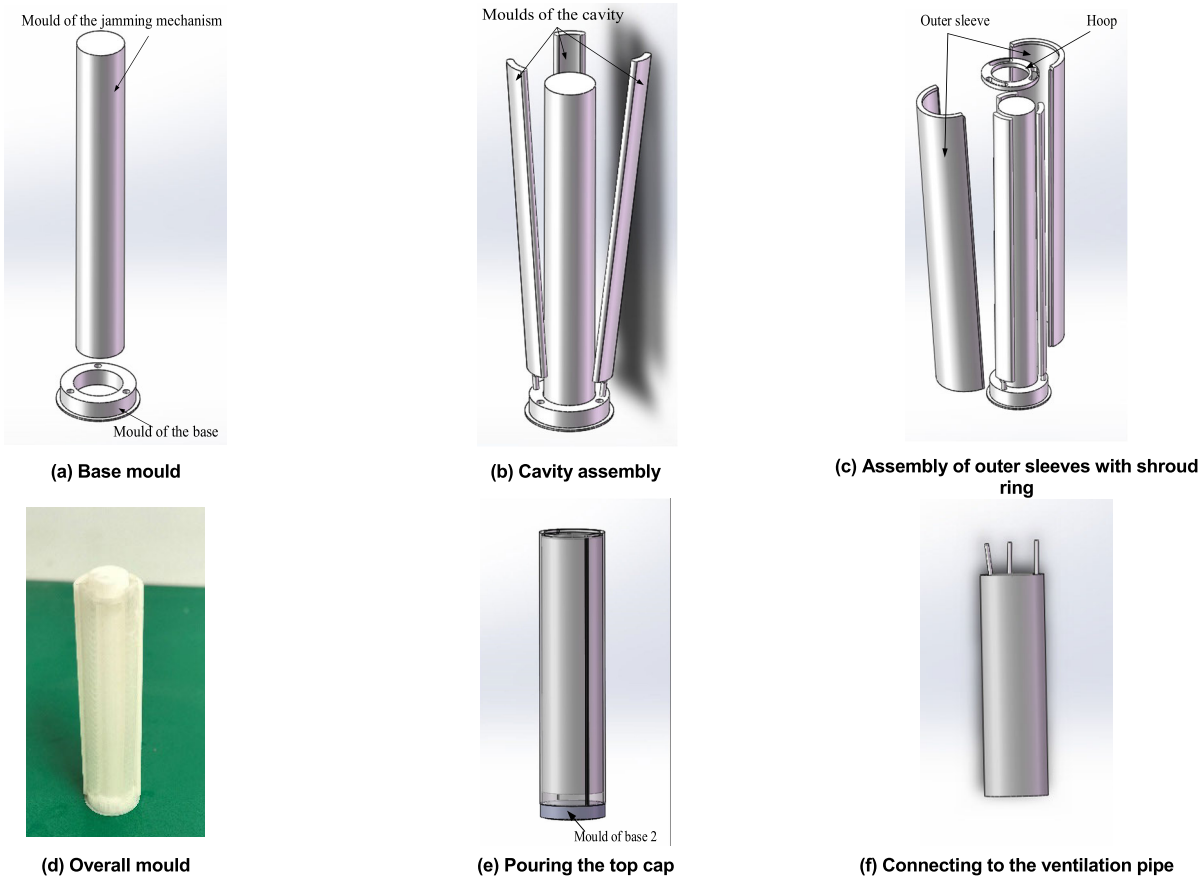

(a) Base mould

(b) Cavity assembly

(c) Assembly of outer sleeves with shroud ring

(d) Overall mould

(e) Pouring the top cap

(f) Connecting to the ventilation pipe

FIGURE 10. Flows for making the soft robot.

A and B, and mixed in A 1:1 (volume ratio) ratio. At room temperature, the curing time is 4 hours. At 60°, the curing time is 30 minutes.After curing, the tensile strength was 200 psi and the fracture elongation was 900%.

Dragon skin 10 silicone material has a shao's hardness of 10A and a mixing viscosity of 23000 cps. It is divided into two groups A and B, which are mixed at the ratio of 1:1 (volume ratio). At room temperature, curing time is 5 hours. At 60°, the curing time was 30 minutes, and the tensile strength after curing was 475 psi.

The liquid silica gel was a Dragon Skin-10 silica gel with an elastic modulus and hardness much higher than those of ECOFLEX-0030.

The pneumatically-driven structure had semi-circular cavities with a wall thickness of 2mm. To facilitate the removal of the mould, the mould was designed using the separation method. After 3-d printing, the assembly was completed according to the flows shown in Figure10: (1) The base was assembled with mould of the jamming mechanism (Figure 10a). (2) The air inlet ends of three moulds for a

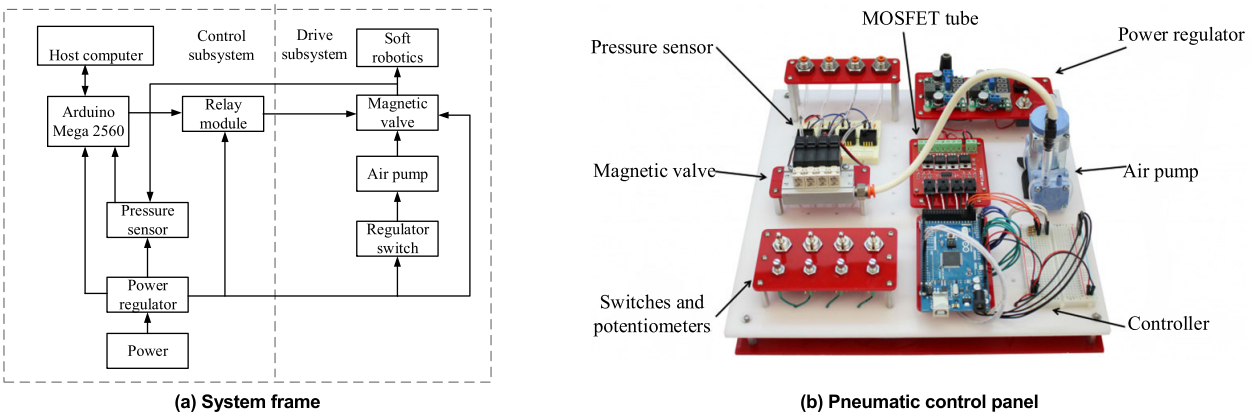

(a) System frame

(b) Pneumatic control panel

FIGURE 11. Pneumatic control system.

cavity were inserted into the base and a gap was reserved (Figure 10b). (3) The mould was sheathed in two outer sleeves and they were assembled and fixed (Figure 10c). (4) The prepared ECOFLEX-0030 silica gel was poured into the mould. (5) The whole mould was heated. After solidifying the silica gel, the base (1) and the moulds of the cavity were removed and the flexible body was flipped. Moreover, the mould of the base (2) was assembled with sleeves (Figure 10e), the outside of which were covered with a sealing film. (6) The prepared Dragon Skin silica gel was poured in the mould, so that the silica gel fills all gaps of the mould, making complete contact with the flexible body. (7) The whole mould was heated and all moulds were removed after solidification. (8) Silica hoses were inserted into small holes of the cavity and 703 silicone rubber was used for adhesive bonding and sealing (Figure 10*f*).

B. REALIZATION OF ROBOT CONTROL SYSTEM

The drive equipment of the robot was the pneumatic control system and a vacuum control system was used to adjust the stiffness of the jamming mechanism.

The pneumatic control system included a control subsystem and a drive subsystem, as shown in Figure 11. The drive subsystem consisted of an air pump (air source), a magnetic valve, and a regulator. A brushless DC micro-diaphragm pump was selected as the air source, which could provide the highest normal pressure of 28psi and vacuum pressure of 25psi. By exchanging inlet and outlet of the air pump, the function can be switched between an air pump and a vacuum pump. An Arduino Mega 2560 microcontroller was used as the control subsystem and a Honeywell 100PGAA5 gas pressure transmitter module was used as the pressure sensor. The module, integrating a signal-processing chip and a digital conditioning chip, could digitally compensate any offset, temperature drift, and non-linearity of the sensor.

The vacuum control system was provided by a FY-1H-N vacuum pump with the maximum vacuum pressure of -101.323kPa, a pumping rate of 1L/s, and an operating power of 150W. An ITV2090-01S5 electric proportional valve under vacuum conditions was selected as the control system.

V. PROPERTIES EXPERIMENTS OF THE SOFT ACTUATOR

The bending and tensile properties of the robot are important indices used to evaluate the pneumatic drive mechanism. Here we studied the repeatable accuracy and stability of the robot by using the method of mathematical statistics (standard deviation, coefficient of variation, and mean absolute deviation) based on bending and tensile tests.

A. TESTING PLATFORM

The designed test platform was composed of a test system and an image monitoring system (Figure 12). The soft actuator was clamped on the support and the three cavities were connected to the control panel through the ventilation pipes. An air source was provided by the air pump that was connected to a host computer, so as to set and monitor pressure parameters.

Due to the rapid deformation response, small offset, and high requirements for accuracy of monitoring data of the soft actuator, the robot vision system was selected for monitoring. The vision system included a high-speed camera and an image processing system (Figure 12b). The high-speed camera was controlled by the host computer to collect image information. After that, the images were imported into the image processing software of the host computer for analysis and processing to obtain spatial coordinates of initial position and marked position of the end of the soft actuator, thus obtaining the bending deformation.

B. STIFFNESS TESTING

The test platform comprised a holder, a support bar, a stepping motor, a digital pressure sensor, and a linear guide. One end of the robot was fixed on the support by a clamping device, while the other end was vertically free, allowing easy adjustment of the height and angle. The measuring end of the digital pressure sensor was fixed on a sliding block of the linear guide, which was driven by the stepping motor and moved horizontally, with a step angle of 1.8° and torque of 0.9N/m. Moreover, the achievable control accuracy was $\pm$ 0.1mm. The digital display pressure sensor was accurate to $\pm$ 0.01N and measuring range was 20N.

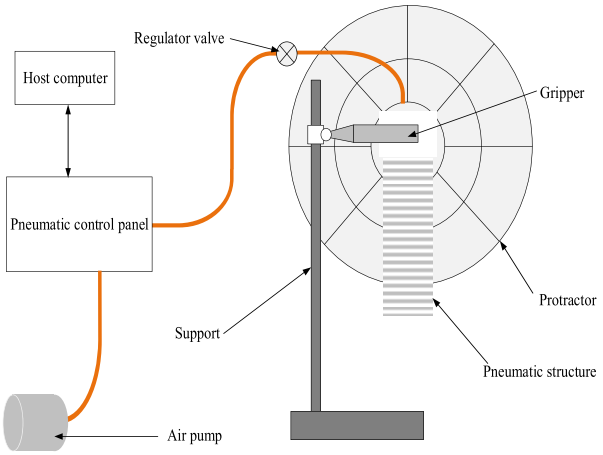

(a) Schematic diagram of the test platform

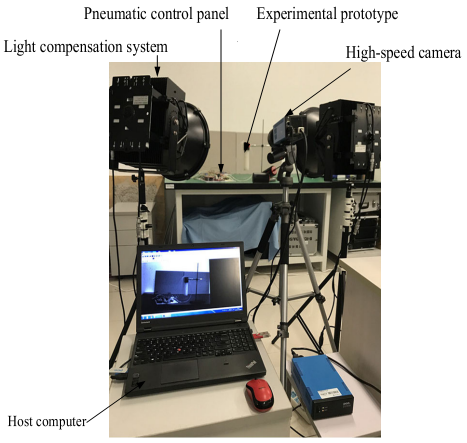

(b) Scene of the test platform

FIGURE 12. Test platform of the soft robot.

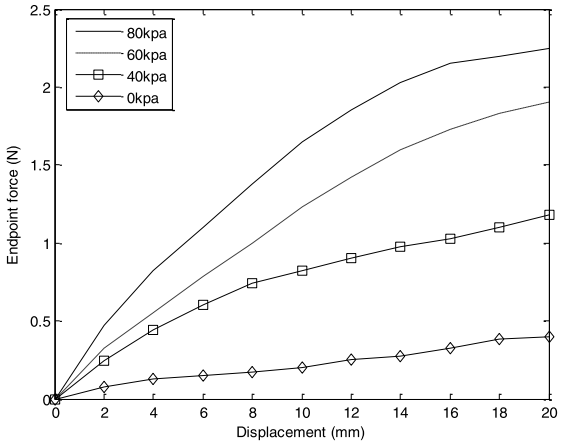

FIGURE 13. The change in endpoint force with displacement under different vacuum conditions.

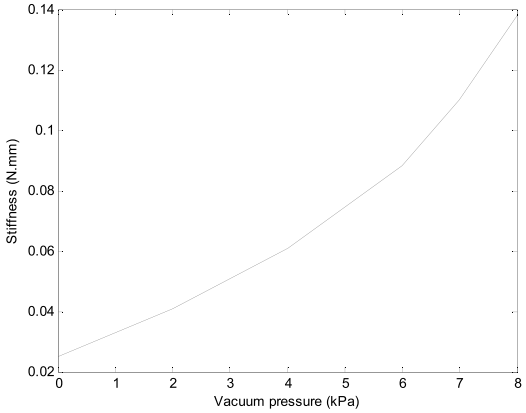

FIGURE 14. Relationship between stiffness at the end of the mechanism and vacuum pressure.

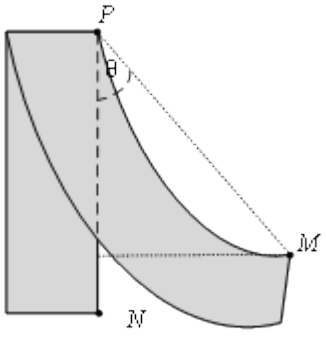

FIGURE 15. Bending angle of pneumatically-driven structure.

In the test process, the end of the robot was in contact with the sensor and the movement distance of the sensor was controlled by the stepping motor over the range of 0-20mm, in 2mm increments. The reading on the sensor was the endpoint force.

By selecting particles with radius of 3mm for filling, the relationship between endpoint force and displacement of the mechanism under different vacuum pressures of 0, 40, 60 and 80kPa was obtained. Four groups of experiments were conducted and each group was repeated for four times to calculate the average results of data obtained (Figure 13).

In the jamming mechanism, the harder the vacuum, the larger the endpoint force measured by the sensor under the same displacement. When the increment in hardness of the vacuum is the same, the increment of endpoint force gradually decreases.

The stiffness K of the robot is given by:

$$k = \frac{f_c}{d_c} \tag{3}$$

where, Fc represents the pressure applied at the end, that is, pressure measured by the sensor; dc indicates the displacement at the end of the robot, namely, displacement of the sliding block on the linear guide. The vacuum pressures are set to 0, 20, 40, 60, 70, and 80kPa and the range of displacement of the sliding block is 0-20mm, moving 2mm at each time. By fitting the experimental data under each group of pressures, the corresponding relationship between stiffness

TABLE 2. Data processing results: bending angles when loaded with a single cavity.

Pressure（kPa）	Average bending angle（°）	Standard deviation of bending angle（°）	Maximum absolute deviation（°）
8	5.955485879	0.38081439	0.783061128
14	16.96842151	1.505611069	2.274035094
18	32.41445745	2.769155709	5.124729139
20	59.0891597	5.397561903	9.159905005

(a) Bending performance

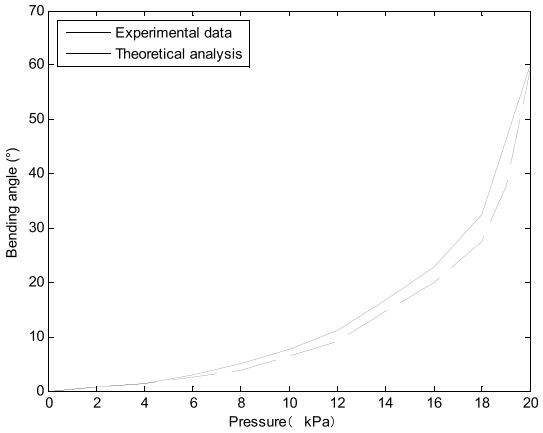

(b) The relationship between bending angle and pressure

FIGURE 16. Driving experiment with a single cavity.

of the robot and the input vacuum pressure was obtained (Figure 14). It can be observed that, with the increase of input vacuum pressure, stiffness of the mechanism gradually rises in the range of 0.025-0.138N/mm and the increase itself also gradually increases.

C. TESTING OF BENDING PERFORMANCE

The bending angle is the angle between the axis of end face and the vertical axis after the soft robot is driven by pressure. We measured the bending angle after loading with single or double cavities on the robot, thus calculating the spatial coordinates (Figure 15): the coordinates of the fixed end (top) is $p = (x_0, y_0)$ and the initial coordinates of the end are $N = (x_1, y_1)$. After being driven by pressures, coordinates of the end are $M = (x_2, y_2)$, so the angle θ of axis of the end of the actuator with the vertical direction can be calculated:

$$\theta = \arctan\left(\frac{x_2 - x_1}{y_2 - y_1}\right) \tag{4}$$

1) DRIVING EXPERIMENT WITH A SINGLE CAVITY

The test is shown in Figure 16a. Pressures in the range of 0-20kPa were applied, bending deformation of the soft actuator was observed, and the bending angle calculated. By repeating 30 groups of tests, the average value under each pressure was obtained to establish the relationship between

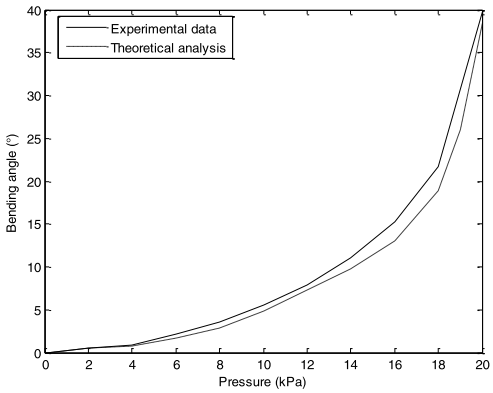

FIGURE 17. The relationship between bending angle and pressure.

bending angle and pressure (Figure 16b). Therefore, the theoretical results (Figure 6) showed a similar trend in deformation. Furthermore, values in this theoretical analysis were smaller than the measured data, while the maximum ratio of the difference to the actual measurement is only 17.91%, thus the experimental results could be deemed to match theoretical values.

To study the stability performance of the robot, driving pressures corresponding to bending angles of 5°, 16°, 32°, 60° were selected and statistics (Supplementary Table 1) corresponding to these pressures were summarised (Table 2):

(a) Loading experiment: single cavity

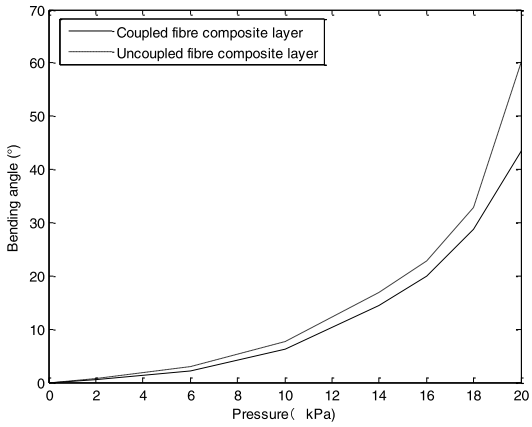

(b) The relationship between bending angle and pressure

FIGURE 18. Bending test of the actuator coupled with a fibre composite layer.

TABLE 3. Statistical analysis: bending angles when loaded with double cavities.

Pressure（kPa）	Average bending angle（°）	Standard deviation of bending angle (°)	Maximum absolute deviation (°)
10	5.664590767	0.403471155	0.766823972
16	15.4080343	1.086687167	2.031775827
20	39.74837808	3.28099532	6.490431748

with the increase of pressure in the cavity, the standard deviation of the data increases, indicating that positioning accuracy of the bending (bending angle) of the mechanism decreases; however, under the pressures selected in this study, the coefficient of variation is within 10%, proving that the mechanism has good stability and high repeatable accuracy. In the meanwhile, under the pressures of 8, 14, 18, 20kPa, the maximum absolute deviations (repeatable accuracy) of bending angles are 0.783061128°, 2.274305094°, 5.124729139°, 9.159905005°. The data suggest that, as the pressure rises, the repeatable accuracy of bending angle of the mechanism gradually decreases, indicating that this pneumatic mechanism is more suitable for low-pressure-driven applications.

2) DRIVING EXPERIMENT WITH DOUBLE CAVITIES

Pressure was simultaneously applied to double cavities of the soft actuator to drive the soft actuator and the range of pressures was set to 0-20 kPa. By repeating 30 groups of the experiments, the relationship between average bending angle and pressure can be obtained (Figure 17). It can be observed that, with increasing pressure, the bending angle of the mechanism gradually rises and slope of the curve rises. By comparing the data measured in the experiment with theoretical results in Figure 8, the theoretical results are seen to have been slightly smaller than the experimental results and the maximum ratio of difference to the actual measurement is only 18.71%, indicating that the theoretical analysis is consistent with the experimental results.

To verify the stability of the mechanism while applying pressure to double cavities, statistical analysis of the data was undertaken (Supplementary Table 2) after tests at pressures of 10kPa, 16kPa, 20kPa, as shown in Table 3. As the pressure in the cavities increased, the standard deviation of the bending angles increased, indicating that the stability of the system gradually decreased. From the perspective of the maximum absolute deviation, the maximum absolute deviations were 0.766823972°, 2.031775827°, 6.490431748° at pressures of 10kPa, 16kPa, 20kPa. The data show that the maximum deviation of bending angles of the whole mechanism increases with the pressure. When double cavities are inflated, the ratio (16.3%) of the maximum absolute deviation to the average bending angle is slightly larger than that (15.4%) when pressure is applied to a single cavity. The repeatable accuracy of the driving of the mechanism with double cavities is slightly lower than that when driving it with a single cavity.

3) TESTS OF BENDING PERFORMANCE OF THE MECHANISM COUPLED WITH THE FIBRE COMPOSITE LAYER

By applying pressure to a single cavity in a soft actuator coupled with a fibre composite layer (Figure 18a) in the range of 0-20 kPa, the relationship between bending angle and pressure was established and compared with that shown

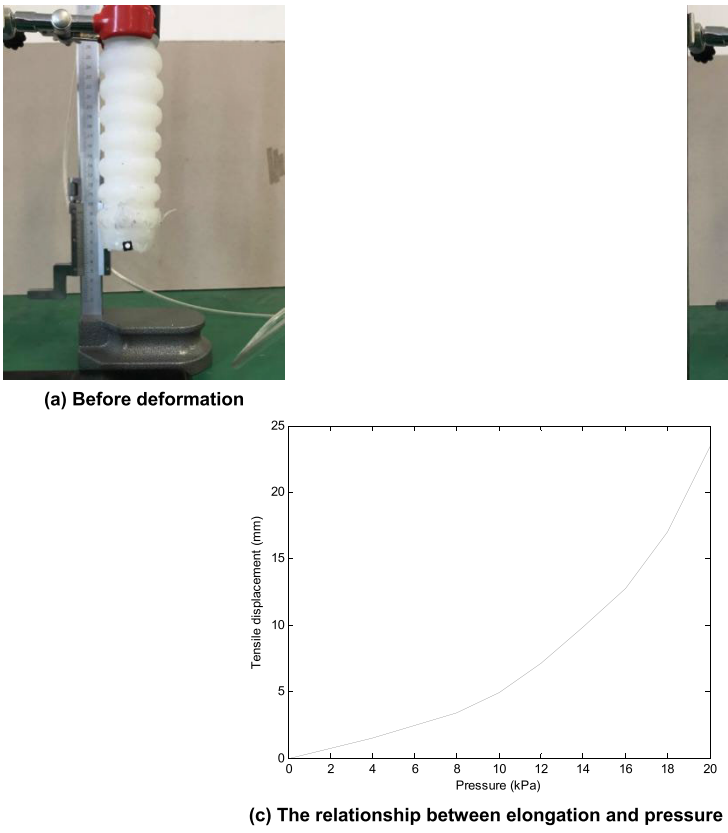

FIGURE 19. Elongation testing of the mechanism.

TABLE 4. Statistical analysis: elongation test data.

Pressure（kPa）	Average elongation（mm）	Standard deviation（mm）	Maximum absolute deviation（mm）
10	4.927592394	0.251534151	0.522797366
18	17.33067963	1.407854093	2.906800323
20	23.50129668	1.886266129	4.092518376

in Figure 15, as shown in Figure 18b. It can be seen that bending performance of the robot coupled with the fibre composite layer is slightly inferior to that of the uncoupled mechanism and is more similar to the results as predicted by theoretical analysis.

D. ELONGATION PERFORMANCE TESTING OF THE SOFT ROBOT

By applying pressure to the three cavities in the pneumatically-driven structure (Figure 19) in the range from 0-20kPa, 20 groups of experiments were repeated to establish the relationship between elongation (average) at the end and pressure (Figure 19c). With increasing pressure, the elongation gradually rises and the higher the pressure, the more sensitive the elongation to changes in pressure.

To verify the stability of the elongation performance of the actuator, according to average elongation, data (Supplementary Table 3) collected at pressures of 8,18,20kPa were selected for statistical processing. Based on this, the standard deviation and coefficient of variation of the data were calculated (Table 4). With increased pressure in the cavities, the standard deviation of the data set increased: the higher the standard deviation, the lower the stability of the system. At 8,18,20kPa, the maximum absolute deviations were 0.522797366mm, 2.906800323mm, 4.092518376mm, indicating that the maximum deviation of bending angle of the overall mechanism rises with increasing pressure.

VI. CONCLUSIONS

In this paper, we developed a soft actuator model for a soft robot with real-time variable stiffness by combining the advantages of Pneu-Net structure and the driven jamming mechanism. Through using the finite element method, we analysed the motion characteristics of the Pneu-Net

SUPPLEMENTARY TABLE 1. Bending angles after inflating a single cavity.

Number of times	Bending angle at 8kPa (°)	Bending angle at 14kPa (°)	Bending angle at 18kPa (°)	Bending angle at 20kPa(°)
1	5.230955844	16.77140457	33.13739468	59.66278381
2	5.965647918	17.92927024	36.16099994	67.69270829
3	5.262076808	16.06135764	33.89009568	62.94598027
4	5.649631755	15.7657357	29.72783451	54.32699082
5	5.63896455	15.59409501	29.42907654	53.39141271
6	5.788966337	15.29612182	29.37149276	52.95076719
7	5.970241957	14.69811793	27.925768	51.34598027
8	5.85540128	16.70986535	32.41627366	57.39097461
9	6.068497838	15.94801096	29.03537249	52.46598027
10	5.480752613	16.70986535	29.1015918	53.26593027
11	5.813802366	17.72821544	33.78545707	59.72278381
12	6.012633386	18.08135776	33.56014942	59.29825328
13	6.145965949	16.3895436	29.78736285	52.74437265
14	5.90464108	16.53707593	29.32977413	52.9107734
15	6.738547008	18.82906875	36.94227615	66.00189293
16	6.509692701	15.71736214	30.29872497	53.91077461
17	5.665453935	15.00158509	29.43654375	52.09097461
18	6.595076519	18.88994847	36.1041139	67.50983187
19	6.455192014	18.00006504	32.66798397	61.42598027
20	6.127406925	18.66067591	37.53918659	68.24906471
21	6.298767817	16.87425843	33.23783301	60.88397425
22	6.210061253	15.14371669	28.64783396	53.71921303
23	5.856412225	17.85380933	33.60402283	58.42711816
24	5.830786302	17.16090398	32.68205023	60.78073668
25	6.175510219	18.5025551	33.01796739	62.50411157
26	6.105295662	18.04137782	32.96674387	61.39041972
27	5.844711354	18.0166172	33.66588915	62.51079054
28	5.502006109	17.30674631	34.53843922	63.88913295
29	5.492471156	16.85501155	33.54609908	62.29066416
30	6.469005501	18.09085163	36.87937201	66.97441932

SUPPLEMENTARY TABLE 2. Bending angles after inflating the double cavities.

Number of times	Bending angle at 10kPa (°)	Bending angle at 16kPa (°)	Bending angle at 20kPa (°)
1	6.261768884	15.80580209	42.3865529
2	5.996725255	16.6309093	44.39034605
3	4.974287667	13.37625847	33.25794633
4	5.327202734	13.73521984	34.47920923
5	5.622891892	13.96505144	35.92241686
6	5.05088275	13.5867457	37.18574815
7	6.170482903	15.27853076	35.34685953

SUPPLEMENTARY TABLE 2. ***Continued.*** **Bending angles after inflating the double cavities.**

8	5.931882011	15.26897306	40.78772112
9	6.431414739	16.9357393	38.6546267
10	5.756390154	14.71054653	34.93486179
11	5.115136365	16.10300108	40.56844899
12	5.586899542	16.38605432	37.73141002
13	5.771268464	14.1584347	36.79517311
14	5.163800478	14.64388578	37.82631421
15	5.928099028	14.0784891	45.67260838
16	6.06980749	16.64440796	38.26420864
17	5.489962748	14.43481985	38.53327585
18	5.998700603	16.60177485	42.49176092
19	5.273339328	15.9542367	40.44481229
20	5.543678011	14.95215073	44.21905428
21	6.211750459	16.83428433	39.01348435
22	5.460075517	14.5386982	36.57967882
23	5.829008858	15.72242242	42.05325323
24	5.447159774	14.89636505	40.60254876
25	6.298711223	16.23894423	41.87131114
26	5.35172918	15.81714518	41.90632227
27	5.168173314	16.60893226	42.51974769
28	5.70570982	15.76733913	41.9327203
29	5.377344132	15.76338287	41.63776342
30	5.623439692	16.80248378	44.44115703

SUPPLEMENTARY TABLE 3. **Elongations after inflating the three cavities.**

Number of times	Elongation at 8kPa (mm)	Elongation at 18kPa (mm)	Elongation at 20kPa (mm)
1	5.21619624	16.36658284	21.570896
2	4.49500496	19.96703752	26.8767648
3	5.35792176	15.68756002	21.2467528
4	5.194836923	14.42387931	20.2805192
5	4.89038904	16.06830764	22.14172692
6	4.875243397	18.77478482	25.01331924
7	4.67532432	14.73615433	19.40877831
8	4.95168848	17.20967291	22.60895515
9	4.95792248	19.12627291	25.30078026
10	4.81038976	19.13904595	24.8561708
11	5.45038976	16.90188664	22.71865392
12	5.14285704	17.37621958	24.58309033
13	4.974847013	17.05611687	22.98386731
14	4.558005092	17.79356766	24.12301109
15	4.892985616	17.47234261	24.56593267
16	4.835613246	17.71687484	25.26267604
17	4.950187525	17.26600043	23.82124733
18	4.827334587	18.08571302	24.4364875
19	4.902945986	17.41972992	23.14534957
20	4.591764651	18.02584283	25.08095448

structure and influences of pressure in its cavities as well as the shape and size of such cavities on the bending and motion performances of a soft robot. Theoretical analysis and experimental results demonstrate that the soft robot can realise a variable stiffness of between 0.025-0.138 N/mm. When bending deformation occurs, at bending angles of between 0-40°, the coefficient of variation remains within 10%, indicating that the mechanism provided good stability and a high, repeatable accuracy. At pressures of less than 14 kPa, the maximum absolute deviation (repeatable accuracy) of the bending angle is less than 2.27°; however, with increasing pressure, the repeatable accuracy of the bending angles of the mechanism gradually decreases. In accordance with statistical analysis, the repeatable accuracy when driving the robot via a single cavity is higher than that when driving it via double cavities, suggesting that this pneumatic mechanism is more suitable for low-pressure-driven applications.

VII. APPENDIX

See Supplementary Tables 1–3.

REFERENCES

[1] H. Shen, "Meet the soft, cuddly robots of the future, Rigid robots step aside—A new generation of squishy, stretchy machines is wiggling our way," *Nature*, vol. 530, pp. 24–26, Feb. 2016.
[2] B. Mosadegh, P. Polygerinos, C. Keplinger, S. Wennstedt, R. F. Shepherd, U. Gupta, J. Shim, K. Bertoldi, C. J. Walsh, and G. M. Whitesides, "Pneumatic networks for soft robotics that actuate rapidly," *Adv. Funct. Mater.*, vol. 24, no. 15, pp. 2163–2170, Apr. 2014.
[3] R. Deimel and O. Brock, "A novel type of compliant and underactuated robotic hand for dexterous grasping," *Int. J. Robot. Res.*, vol. 35, nos. 1–3, pp. 161–185, Jan. 2016.
[4] D. Rus and M. T. Tolley, "Design, fabrication and control of soft robots," *Nature*, vol. 521, no. 7553, pp. 467–475, May 2015.
[5] F. Saunders, B. A. Trimmer, and J. Rife, "Modeling locomotion of a soft-bodied arthropod using inverse dynamics," *Bioinspiration Biomimetics*, vol. 6, no. 1, Mar. 2011, Art. no. 016001.
[6] Y. Shapiro, K. Gabor, and A. Wolf, "Modeling a hyperflexible planar bending actuator as an inextensible Euler–Bernoulli beam for use in flexible robots," *Soft Robot.*, vol. 2, no. 2, pp. 71–79, Jun. 2015.
[7] C. Majidi, R. F. Shepherd, R. K. Kramer, G. M. Whitesides, and R. J. Wood, "Influence of surface traction on soft robot undulation," *Int. J. Robot. Res.*, vol. 32, no. 13, pp. 1577–1584, Nov. 2013.
[8] B. A. Jones and I. D. Walker, "Kinematics for multisection continuum robots," *IEEE Trans. Robot.*, vol. 22, no. 1, pp. 43–55, Feb. 2006.
[9] E. Yahya, V. Augusto, and L. Constantina, "Finite element analysis and design optimization of a pneumatically actuating silicone module for robotic surgery applications," *Soft Robot.*, vol. 1, no. 4, pp. 1–8, Dec. 2014.
[10] Y. Elsayed, C. Lekakou, T. Geng, and C. M. Saaj, "Design optimisation of soft silicone pneumatic actuators using finite element analysis," in *Proc. IEEE/ASME Int. Conf. Adv. Intell. Mechatronics*, Jul. 2014, pp. 44–49.
[11] Y. Hongliang, X. Fengyu, and Y. Yudong, "Design and analysis of variable stiffness soft manipulator based on jamming mechanism," in *Proc. IEEE Int. Conf. Robot. Biomimetics (ROBIO)*, Dec. 2017, pp. 1–6.
[12] J. Wang, Y. Fei, and Z. Liu, "Locomotion modeling of a triangular closed-chain soft rolling robot," *Mechatronics*, vol. 57, pp. 150–163, Feb. 2019.
[13] N. Tan, X. Gu, and H. Ren, "Pose characterization and analysis of soft continuum robots with modeling uncertainties based on interval arithmetic," *IEEE Trans. Autom. Sci. Eng.*, vol. 16, no. 2, pp. 570–584, Apr. 2019.
[14] S. Wakimoto, K. Suzumori, and K. Ogura, "Miniature pneumatic curling rubber actuator generating bidirectional motion with one air-supply tube," *Adv. Robot.*, vol. 25, nos. 9–10, pp. 1311–1330, Jan. 2011.
[15] P. Polygerinos, Z. Wang, J. T. B. Overvelde, K. C. Galloway, R. J. Wood, K. Bertoldi, and C. J. Walsh, "Modeling of soft fiber-reinforced bending actuators," *IEEE Trans. Robot.*, vol. 31, no. 3, pp. 778–789, Jun. 2015.
[16] G. Agarwal, N. Besuchet, B. Audergon, and J. Paik, "Stretchable materials for robust soft actuators towards assistive wearable devices," *Sci. Rep.*, vol. 6, no. 1, 2016, Art. no. 34224.
[17] G. Udupa, P. Sreedharan, P. S. Dinesh, and D. Kim, "Asymmetric bellow flexible pneumatic actuator for miniature robotic soft gripper," *J. Robot.*, vol. 2014, pp. 1–11, Dec. 2014.
[18] F. Meng, F. Xu, M. Wu, and G. Jiang, "Modeling and experiment of three-cavity soft manipulator," in *Proc. 5th IEEE Int. Conf. Cloud Comput. Intell. Syst. (CCIS)*, Nanjing, China, Nov. 2018, pp. 1018–1022.
[19] Y. Yudong, X. Fengyu, Y. Hongliang, and Z. Pengfei, "A rolling soft cable climbing robot: Design analysis and fabrication," in *Proc. IEEE Int. Conf. Robot. Biomimetics (ROBIO)*, Dec. 2017, pp. 1–6.
[20] Y. Wei, Y. Chen, Y. Yang, and Y. Li, "A soft robotic spine with tunable stiffness based on integrated ball joint and particle jamming," *Mechatronics*, vol. 33, pp. 84–92, Feb. 2016.
[21] A. Jiang, T. Ranzani, G. Gerboni, L. Lekstutyte, K. Althoefer, P. Dasgupta, and T. Nanayakkara, "Robotic granular jamming: Does the membrane matter?" *Soft Robot.*, vol. 1, no. 3, pp. 192–201, Sep. 2014.
[22] A. J. Loeve, O. S. Van De Ven, J. G. Vogel, P. Breedveld, and J. Dankelman, "Vacuum packed particles as flexible endoscope guides with controllable rigidity," *Granular Matter*, vol. 12, no. 6, pp. 543–554, Dec. 2010.
[23] Y. Yang, Y. Chen, Y. Li, M. Z. Chen, and Y. Wei, "Bioinspired robotic fingers based on pneumatic actuator and 3D printing of smart material," *Soft Robot.*, vol. 4, no. 2, pp. 147–162, Jun. 2017.
[24] J. R. Amend, E. Brown, N. Rodenberg, H. M. Jaeger, and H. Lipson, "A positive pressure universal gripper based on the jamming of granular material," *IEEE Trans. Robot.*, vol. 28, no. 2, pp. 341–350, Apr. 2012.
[25] M. Manti, V. Cacucciolo, and M. Cianchetti, "Stiffening in soft robotics: A review of the state of the art," *IEEE Robot. Automat. Mag.*, vol. 23, no. 3, pp. 93–106, Sep. 2016.
[26] J. Wang, Y. Fei, and W. Pang, "Design, modeling, and testing of a soft pneumatic glove with segmented PneuNets bending actuators," *IEEE/ASME Trans. Mechatronics*, vol. 24, no. 3, pp. 990–1001, Jun. 2019.
[27] T. Ranzani, M. Cianchetti, G. Gerboni, I. D. Falco, and A. Menciassi, "A soft modular manipulator for minimally invasive surgery: Design and characterization of a single module," *IEEE Trans. Robot.*, vol. 32, no. 1, pp. 187–200, Feb. 2016.
[28] J. Bao, W. Chen, and J. Xu, "Kinematics modeling of a twisted and coiled polymer-based elastomer soft robot," *IEEE Access*, vol. 7, no. 2, pp. 136792–136800, 2019.
[29] Z. Zhang, X. Wang, S. Wang, D. Meng, and B. Liang, "Design and modeling of a parallel-pipe-crawling pneumatic soft robot," *IEEE Access*, vol. 7, pp. 134301–134317, 2019.
[30] M.-G. Zhang, Y.-P. Cao, G.-Y. Li, and X.-Q. Feng, "Spherical indentation method for determining the constitutive parameters of hyperelastic soft materials," *Biomech. Model. Mechanobiol.*, vol. 13, no. 1, pp. 1–11, Jan. 2014.
[31] Y. Elsayed, A. Vincensi, C. Lekakou, T. Geng, C. M. Saaj, T. Ranzani, M. Cianchetti, and A. Menciassi, "Finite element analysis and design optimization of a pneumatically actuating silicone module for robotic surgery applications," *Soft Robot.*, vol. 1, no. 4, pp. 255–262, Dec. 2014.

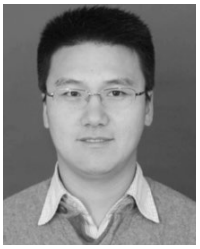

FENG-YU XU received the B.S. degree in mechanical engineering from the Changchun University of Technology, Changchu, China, in 2002, the M.S. degree from the Hefei University of Technology, in 2005, and the Ph.D. degree from Southeast University, in 2009. From 2009 to 2012, he was a Postdoctoral Research Fellow with the School of Automation, Institute of Intelligent Robotics and Intelligent Control, Southeast University, Nanjing, China. From 2016 to 2017, he was a Visiting Scholar with the Department of Electrical and Computer Engineering, Michigan State University, East Lansing, MI, USA. He was a Professor of automation engineering with the Nanjing University of Posts and Telecommunications. His main academic interest and research fields are soft robotics, field robotics, biomimetic robot, medical machinery, mechanical design, and mechatronics. His research interests include soft robotics and special climbing robotics.

FENG-YOU JIANG received the bachelor's degree from the School of Mechanical and Electronic Engineering, East China University of Technology, Jiangxi, China, in June 2018. He is currently pursuing the master's degree in automation engineering with the Nanjing University of Posts and Telecommunications. His research interests include soft robotics and special grasping robotics.

QUAN-SHENG JIANG received the Ph.D. degree in mechanical manufacturing and automation from Southeast University, Jiangsu, China, in April 2009. He is currently an Associate Professor and a Master's Supervisor with the School of Mechanical Engineering, Suzhou University of Science and Technology, Jiangsu. He is mainly engaged in intelligent equipment condition monitoring and fault diagnosis research work, including complex mechanical and electrical equipment non-linear fault diagnosis method, and robotics and automation technology.

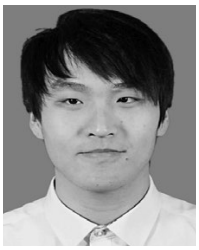

YU-XUAN LU received the bachelor's degree from the School of Electrical Engineering and Automation, Nanhang Jincheng College, China, in June 2018. He is currently pursuing the master's degree in automation engineering with the Nanjing University of Posts and Telecommunications. His research interests include soft robotics and dynamic model of soft robot.